Mechanically flexible waveguide arrays for optical chip-to-chip coupling

Peters, Tjitte-Jelte; Tichem, Marcel

DOI
10.1117/12.2205227

Publication date
2016

Document Version
Final published version

Published in
Proceedings of SPIE OPTO 2016 MOEMS and Miniaturized Systems XV

PROCEEDINGS OF SPIE

SPIEDigitalLibrary.org/conference-proceedings-of-spie

Mechanically flexible waveguide arrays for optical chip-to-chip coupling

Tjitte-Jelte Peters
Marcel Tichem

SPIE.

Mechanically flexible waveguide arrays for optical chip-to-chip coupling

Tjitte-Jelte Peters and Marcel Tichem

Delft University of Technology, Mekelweg 2, Delft, Netherlands

ABSTRACT

This paper reports on the progress related to a multichannel photonic alignment concept, which aims to achieve submicrometer alignment of the waveguides of two photonic integrated circuits (PICs). The concept consists of two steps: chip-to-chip positioning and fixing provide a coarse alignment after which waveguide-to-waveguide positioning and fixing result in a fine alignment. For the waveguide-to-waveguide alignment, mechanically flexible waveguides are used. Positioning of the waveguides is performed by integrated MEMS actuators. The flexible waveguides and the actuators are both integrated in one of the PICs. This paper reports on the fabrication and the mechanical characterization of the suspended waveguide structures.

The flexible waveguide array is created in a PIC which is based on TriPleX technology, i.e. a silicon nitride (Si_3N_4) core encapsulated in a silicon dioxide (SiO_2) cladding. The realized flexible waveguide structures consist of parallel cantilevered waveguide beams and a crossbar that connects the free ends of the waveguide beams. The fabrication of suspended structures consisting of a thick, i.e. 15 µm, TriPleX layer stack is challenged by the compressive mean stress in the SiO_2.

We have developed a fabrication method for the reliable release of flexible TriPleX structures, resulting in a 96 % yield of cantilever beams. The realized suspended waveguide arrays have a natural out-of-plane deformation, which is studied using white light interferometry. Suspended waveguide beams reveal a downward slope at the base of the beams close to 0.5°. In addition to this slope, the beams have a concave upward profile. The constant curvature over the length of the waveguide beams is measured to range from 0.2 µm to 0.8 µm. The profiles measured over the length of the crossbars do not seem to follow a circular curvature. The variation in deflection within crossbars is measured to be smaller than 0.2 µm.

Keywords: Photonics, alignment, waveguides, fabrication, bending, characterization

1. INTRODUCTION

The packaging of PICs is essential to let them interact with their environment. Photonic packaging usually involves creating optical as well as electrical connections. While established methods are available for making electrical connections, e.g. wirebonding and flip-chip bonding,[1] the solutions for optical interconnects are not so well developed.[2] Packaging amounts to a substantial part of the cost in silicon photonics[3] as well as indium phosphide (InP) PICs.[4] For example, the large investment required for a customized robotic assembly system and the substantial operation time until obtaining the final alignment result in high packaging costs.

In previous work,[5] an alignment concept was proposed that eliminates the need for expensive robotic assembly solutions. The three key functions of this alignment concept are (1) mechanically flexible SiO_2 waveguide arrays, (2) positioning by integrated microelectromechanical system (MEMS) functionality, and (3) a fixing method to maintain the optimal alignment. This paper reports on the progress regarding the first key function: mechanically flexible waveguide arrays. The fabrication of suspended SiO_2 beams comes with the risk of beam fracturing, due to the compressive mean stress in the SiO_2. This paper describes a fabrication process for the release of suspended SiO_2 beams with a reduced risk of beam fracturing. Once released, suspended SiO_2 beams deform due to residual stress. Two effects can be distinguished in the deformation of suspended SiO_2 cantilevers.[6,7] The

Further author information: (Send correspondence to M. Tichem)
M. Tichem: E-mail: m.tichem@tudelft.nl
T. Peters: E-mail: t.j.peters@tudelft.nl

MOEMS and Miniaturized Systems XV, edited by Wibool Piyawattanametha, Yong-Hwa Park, Proc. of SPIE Vol. 9760, 97600D · © 2016 SPIE
CCC code: 0277-786X/16/$18 · doi: 10.1117/12.2205227

first deformation is a slope at the cantilever base, also referred to as 'tilt'. The second effect is a an out-of-plane deformation with a constant radius of curvature, also referred to as 'curl'. Both effects are analyzed as part of the mechanical characterization of realized structures.

This article is organized as follows. Section 2 describes the alignment concept. The fabrication process of the mechanically flexible waveguide arrays is explained in section 3. Section 4 describes the mechanical characterization of the realized structures in terms of yield and initial deformation measurements. Our conclusions are summarized in section 5, as well as the prospects resulting from our findings.

2. ALIGNMENT CONCEPT

Our proposed alignment concept aims to achieve optical chip-to-chip alignment with submicrometer accuracy. The alignment configuration of an InP PIC with a TriPleX interposer chip is used to illustrate the concept. Integrated functionality for waveguide-to-waveguide alignment is created within the TriPleX interposer chip. The three key functions that are combined in the integrated alignment functionality are described in more detail in section 2.1. Section 2.2 explains how the optimal alignment is obtained in two steps: a pre-alignment followed by a fine alignment.

2.1 Key functions of the alignment concept

The first function is a mechanically flexible waveguide array. The mechanical flexibility is required in order to position the free end of the waveguide array with respect to the rest of the PIC. The flexible arrays are designed with a minimum beam thickness and width of approximately 16 µm, ensuring lossless light propagation. The length and number of waveguide beams within the array determine its bending stiffness.

The second function is a means to position the free end of the flexible waveguide array. For this, we propose to integrate MEMS functionality in the TriPleX chip. Electrothermal micro actuators can be integrated by microfabrication post-processing applied to TriPleX wafers. The post-processing steps must be compatible (e.g., in terms of temperature) with the TriPleX technology. The positioning of the flexible waveguide array falls outside the scope of this paper, but will be included in future work.

The third function is required to maintain the alignment once the optimal alignment is achieved. Possible solutions for fixing the alignment include bonding by adhesives and soldering,[8] and friction-based clamping. All of these methods have advantages and disadvantages, e.g., the post-bonding shift of an adhesive caused by the curing process. Focusing on the flexible waveguide beams, this paper does not go into further detail regarding the fixing method.

2.2 Two-step alignment

The final sub-micrometer alignment is accomplished in two steps. First, positioning and fixing of the PICs provide chip-to-chip alignment with moderate precision, i.e. down to a few micrometer. After this, the mechanical flexibility of the waveguide array is employed for fine alignment, after which the fixing method maintains the alignment.

Figure 1 presents the pre-alignment step, i.e. coarse alignment and fixing. Both PICs are placed on a common substrate with the waveguide side facing the substrate. The PICs are mechanically and electrically connected to the substrate by flip-chip bonding. This alignment step ensures the coarse alignment of the two PICs in all translations and rotations. At this stage, a misalignment of a few micrometers is tolerable in the three directions shown in dashed red, since those directions will be fine-tuned in the second alignment step.

Once the PICs are coarsely aligned, the integrated alignment functionality is used for the fine-alignment. Figure 2 is a schematic representation of the pre-aligned PICs showing the operation of the integrated alignment functionality. For the sake of simplicity, no actuators are included in this figure. The waveguide beams are connected by a crossbar at their free ends. This crossbar ensures an accurate pitch of the waveguides, determined by the photolithography process. Figure 2 illustrates the fine-alignment in the x-direction only. By positioning the crossbar over distance Δx, the alignment of the flexible waveguides with the waveguides of the InP PIC is improved. The integrated alignment functionality can perform two translations and one rotation (illustrated in dashed red in figure 1). The required motion can be achieved by an actuation scheme consisting of three

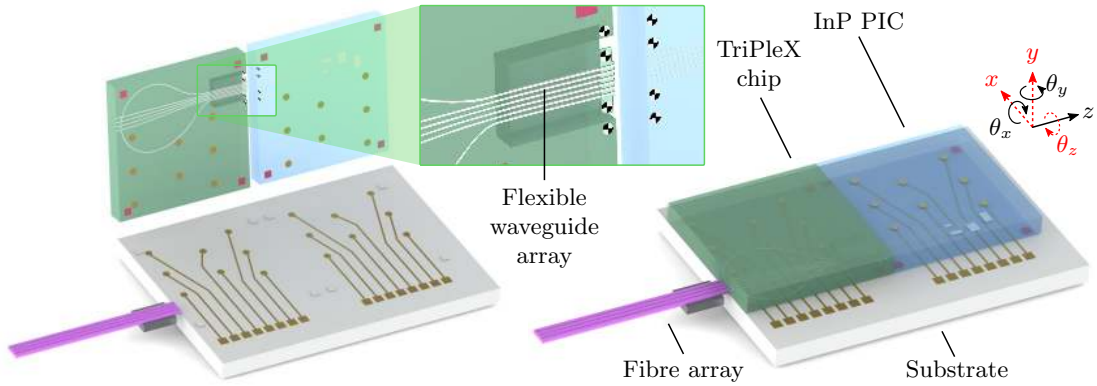

Figure 1. The pre-alignment step of a TriPleX chip and an InP PIC on a common substrate. Left: before assembly, with a view on the waveguide side of the PICs. The inset shows a close-up view of the flexible waveguide array. Right: after assembly, the PICs are mechanically and electrically connected, and the waveguides are pre-aligned.

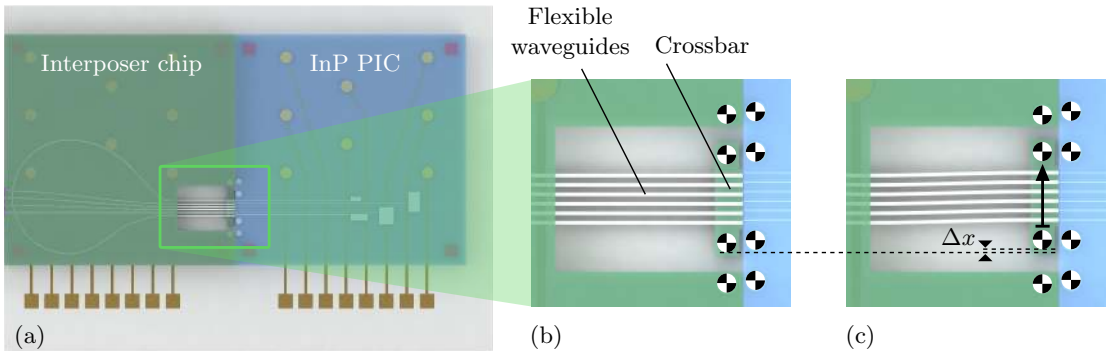

Figure 2. Top view of the fine alignment step, illustrating the fine-alignment in the x-direction. No actuators are shown in this representation.

actuators, as schematically presented in figure 3. The translation in the x direction is achieved by an in-plane actuator on one side of the crossbar. Out-of-plane actuators on both ends of the crossbar control the translation in the y direction, by simultaneously operating both of them. Rotation θ_z is achieved by individually operating the out-of-plane actuators.

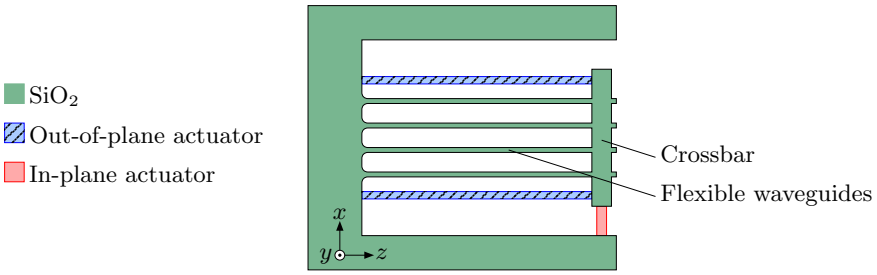

Figure 3. Schematic representation of the actuators for the integrated alignment functionality. The crossbar can be positioned using three actuators. The in-plane actuator provides a translation in the x direction. Simultaneously operating the out-of-plane actuators enables a translation in the y direction. Operating the out-of-plane actuators individually induces a rotation around the z axis.

3. FABRICATION

Two separate microfabrication sequences can be distinguished within the overall fabrication. In the first sequence, a layer stack is added to a silicon (Si) wafer, providing photonic waveguide functionality. On the frontside, this TriPleX layer stack includes Si_3N_4 waveguide cores, embedded in a SiO_2 cladding. A comparable layer stack is

added to the backside of the wafer, to minimize bow and warpage. Because no photonic functionality is required for the backside, only the SiO_2 layers (without Si_3N_4 cores) are deposited there. The fabrication of the embedded waveguides is part of the TriPleX technology,[9] and falls outside the scope of this article.

In the second sequence, waveguide beam arrays are etched in the SiO_2 and released from the substrate. This second sequence can be regarded as post-processing applied to TriPleX wafers, and it is described in more detail below. Figure 4 shows how the entire fabrication process is the combination of fabrication sequence 1 and 2.

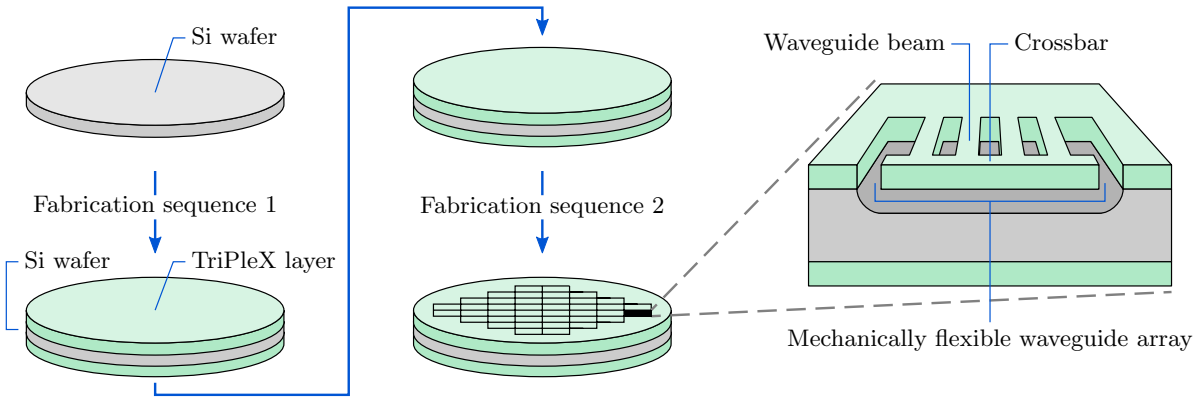

Figure 4. Schematic representation of the fabrication process of mechanically flexible waveguide arrays. Fabrication sequence 2 can be regarded as post-processing after fabrication sequence 1. This article describes the process steps of fabrication sequence 2.

The flexible waveguide arrays are temporarily reinforced by Si during fabrication. This reinforcement prevents the SiO_2 structures from fracturing. More details about the mechanism of the reinforcement method are reported in previous work.[7]

The process steps of fabrication sequence 2 are as follows. The starting material is a Si wafer which is provided with a TriPleX layer (figure 5(a)). A ∼6 µm thick layer of AZ9260 photoresist is spray coated on top of the TriPleX layer and patterned. The mask used in this step is aligned with respect to the Si_3N_4 cores that are embedded in the TriPleX layer. In-plane dimensional parameters like the length and width of the waveguide beams are determined by the design of this photolithography mask. The SiO_2 is plasma etched using a Drytek Triode 384T with C_2F_6–CHF_3 chemistry (figure 5(b)). A pressure of 180 mTorr and 250 W RF power are applied. Without removing the photoresist mask, the same pattern is plasma etched into the Si (figure 5(c)). From this fabrication step on, the etching is performed with an SPTS Omega i2L Rapier deep silicon etcher. A trench depth of ∼100 µm is realized by deep reactive ion etching (DRIE) using SF_6 gas.

With the trenches etched into the Si, a passivation layer consisting of ∼1 µm thick CF_x is deposited using C_4F_8 gas (figure 5(d)). This passivation layer is locally removed from the trench bottom using SF_6 gas and 75 W platen HF power (figure 5(e)). The Si underneath the beams is removed by isotropic plasma etching, while the Si sidewalls are protected by the remaining passivation layer (figure 5(f)). This isotropic etch is performed with SF_6 gas and without any platen HF power. Now that the waveguide array is fully suspended, the Si reinforcement can be removed. The oxygen plasma of a Tepla 300 plasma system strips the passivation layer and the remaining photoresist (figure 5(g)). A similar isotropic plasma etching step as used in (f) removes the supporting Si (figure 5(h)). The end result is a fully suspended waveguide array structure (figure 5(i)). A scanning electron microscope (SEM) image of a realized suspended waveguide array is included as figure 6. The waveguide beams of this particular array are 1000 µm in length and have a mean width of approximately 21 µm. The free ends of the waveguide beams are connected by a crossbar. Etch holes are provided in the crossbar in order to ensure that the waveguide beams do not fracture due to a (temporary) doubly-clamped beam configuration (see previous publication[7] for more details).

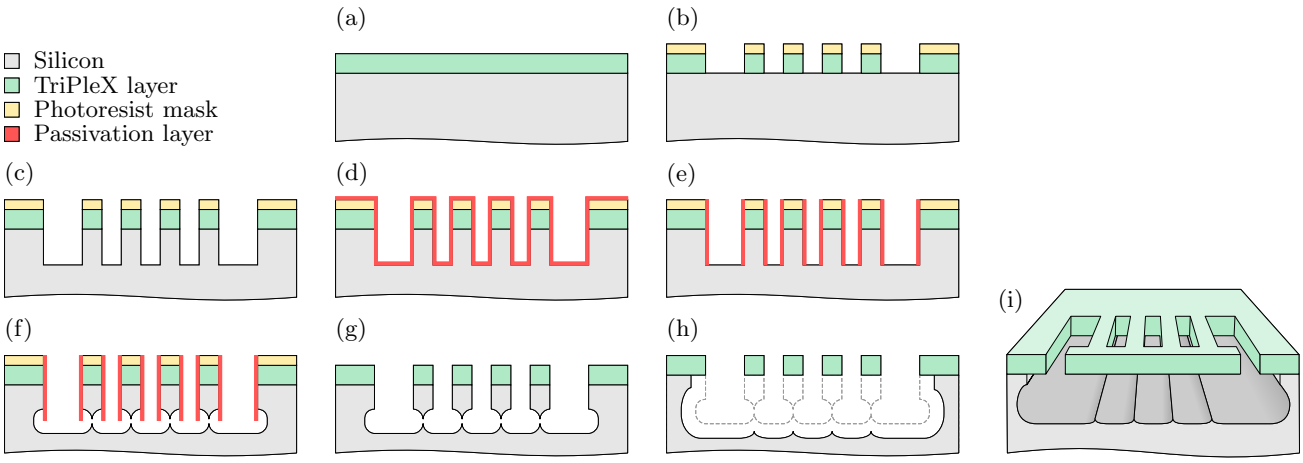

Figure 5. Fabrication steps for mechanically flexible waveguide arrays. This figure only shows the frontside of the wafer. (a) Starting material: Si wafer with TriPleX layer. (b) Photoresist patterning and plasma etching of the TriPleX layer. (c) DRIE of Si. (d) Deposition of passivation layer. (e) Local removal of the passivation layer. (f) Isotropic plasma etching of Si. (g) Removal of passivation layer and photoresist. (h) Isotropic plasma etching of Si. (i) Semi-3D representation of the resulting mechanically flexible waveguide array.

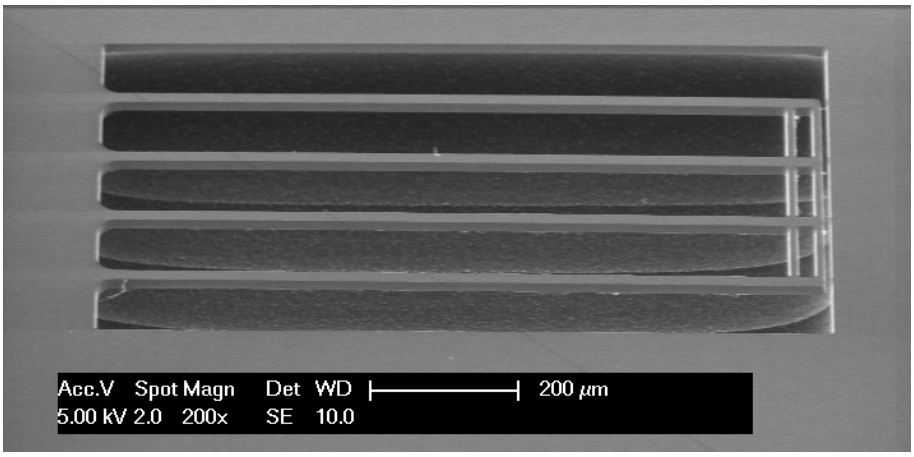

Figure 6. SEM image of a suspended waveguide array. This array includes a crossbar (with etch holes) and four beams that are 1000 µm in length and have a mean beam width of 21 µm.

4. CHARACTERIZATION

The realized waveguide arrays are mechanically characterized. The yield is determined optically and is discussed in section 4.1. White light interferometry is used to obtain a surface height image of the waveguide arrays. The curvature over the length of the waveguide beams is discussed in section 4.2. Section 4.3 includes the curvature measured over the length of the crossbar.

4.1 Yield

The yield is determined by optical inspection. Figure 7 presents the yield of cantilever beams that are approximately 10 µm in width and vary in length. The cantilevers are distributed over 36 dies, with a total number of 4320 cantilevers on a single wafer. For comparison, the yield of cantilevers that were released with and without silicon reinforcement are shown in the same graph. One wafer (with 4320 cantilevers) was inspected after releasing its cantilevers without reinforcement, and another wafer (with 4320 cantilevers) was inspected after releasing its cantilevers with reinforcement. Without silicon reinforcement, all the cantilevers with a length up to 280 µm were intact after release. In contrast, using silicon reinforcement, all the cantilevers with a length up to 750 µm

were intact after release. The overall yield increased from 66 % to 96 %. Furthermore, the yield of the longest cantilevers (1000 µm in length) increased from 20 % to 80 % by using the silicon reinforcement method.

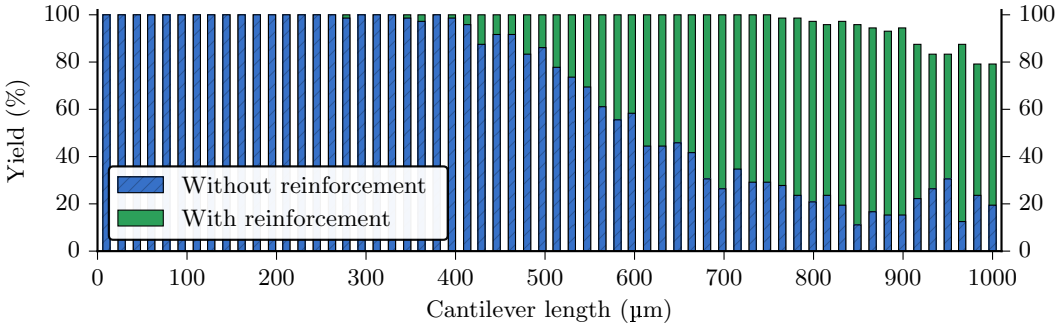

Figure 7. The yield of cantilevers with a constant cross section (width of ∼10 µm and thickness of ∼15.5 µm) as a function of cantilever length. This graph includes both the yield without (shown in blue) and with (shown in green) silicon reinforcement.

4.2 Deflection over the length of the waveguides

A Bruker Contour GT-K 3D optical profilometer was used to obtain deflection profiles over the length of the waveguides. Two types of arrays are measured: one type has separate cantilever beams while the other type has cantilever beams that are connected by a crossbar at their free end. Both types have fillets at the base of the cantilevers in order to reduce stress concentrations. The two different array types are presented schematically in figure 8.

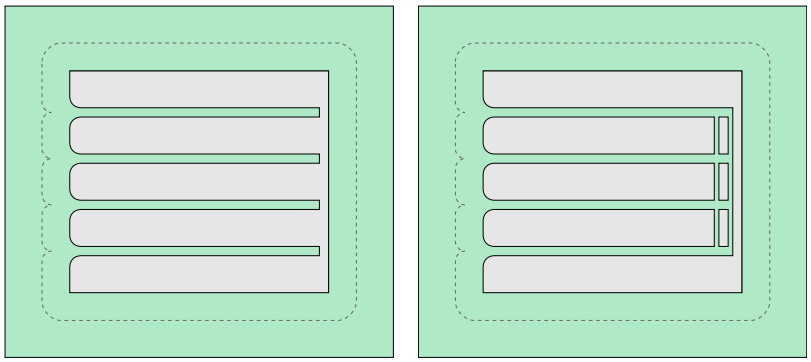

(a) Array type A (b) Array type B

Figure 8. Top view of the two types of waveguide beam arrays. Type A consists of four separate cantilevers. The cantilevers of type B are connected by a crossbar at their free end. The dashed line indicates the boundary of an underetched SiO_2 membrane.

As an example, the deflection profiles of a waveguide beam array consisting of four beams are presented in figure 9. The beams are approximately 750 µm in length and have a mean width of 25 µm. They are of type A, so not connected by a crossbar. The profiles reveal the two expected effects: a slope at the base of the beam and a constant curvature. The most apparent of the two is a downward slope of approximately 0.5° at the base of the beams. This slope causes the free ends to deflect approximately 6 µm towards the substrate. The curvature of the suspended beams is less explicit, but is slightly concave upward for all the beams. The radius of curvature ρ is obtained by curve-fitting a circle over a specific range of every profile (indicated by the dashed vertical lines). The radius values are included in the plots.

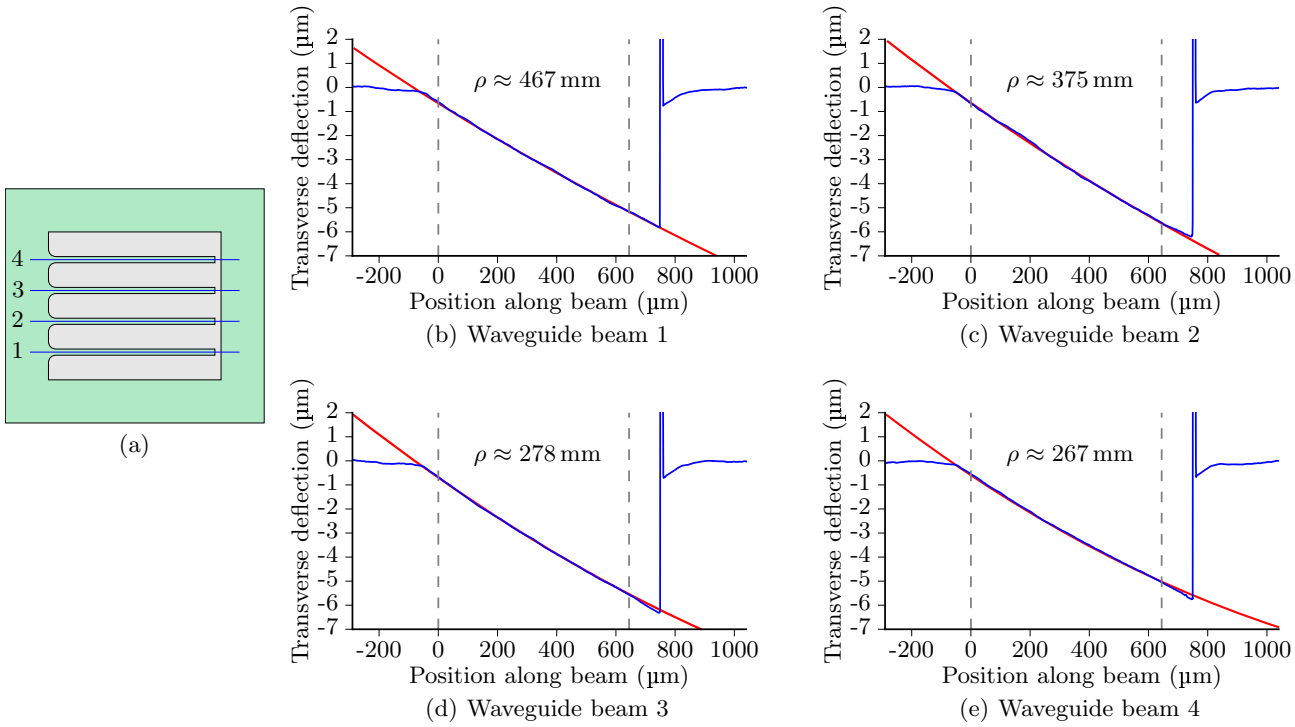

Figure 9. Example deflection profiles measured over the length of four waveguide beams in a single array. (a) shows how the profiles are measured over the length of the beams. The depicted array is of type A and the beams are 750 µm in length and have a mean width of 25 µm. (b)–(e) The deflection profile is presented in blue. In red, a part of a circle is shown. This circle is obtained by curve-fitting the part of the profile between the two dashed vertical lines with a circle.

Using this method, the radius of curvature of 80 beams (20 arrays of four beams each) is determined. Arrays of type A as well as type B are measured, with a designed beam width of 18 µm, 26 µm and 34 µm, beam length of 250 µm, 500 µm, 750 µm and 1000 µm and a pitch of 100 µm. The measured profiles provide a mean value for the radius of curvature of every array, as well as the standard deviation of the four beams within the corresponding array. Besides the measured radius of curvature, the width is an important parameter, because the width determines a beam's bending stiffness, and thus the curvature. Values for the beam width are extracted from the measurement data provided by the optical profilometer. The surface measurements from the profilometer contain information about the top surface of the beams. For every beam, a mean value for the width of this top surface is determined. These values do not represent the actual beam width (the beams have a trapezoidal cross section), but provide a simple quantification of the beam width. Mean width values for every array and the standard deviation of the four beams within the corresponding array are calculated. Figure 10(a) shows the radii of curvature as a function of the waveguide beam width.

The curvature over the length of the suspended beams is concave upward for all the arrays. The data points in figure 10(a) reveal that there is a large spread in the mean values of the radius of curvature, ranging from 0.2 m to 0.8 m. Moreover, certain arrays have a large standard deviation in the radius of curvature (e.g., the array at approximately 24 µm mean beam width).

Considering that the beams mostly consist of SiO_2 (a waveguide beam is a 130 nm thin Si_3N_4 core embedded in a 15.5 µm thick SiO_2 cladding), the curvature results from both intrinsic and extrinsic stress. We make two assumptions. (1) The Si_3N_4 core has negligible dimensional variations (thickness and width). The fabrication of TriPleX waveguides is optimized to provide Si_3N_4 cores with uniform thickness and width. (2) The intrinsic stress is uniform on wafer level. The spread in radius of curvature over arrays in combination with the two assumptions suggest that the SiO_2 thickness varies over the different arrays. A thickness measurement performed before fabrication sequence 2 showed a thickness of 15.5 µm ± 0.7 µm (based on a 5-point wafer measurement).

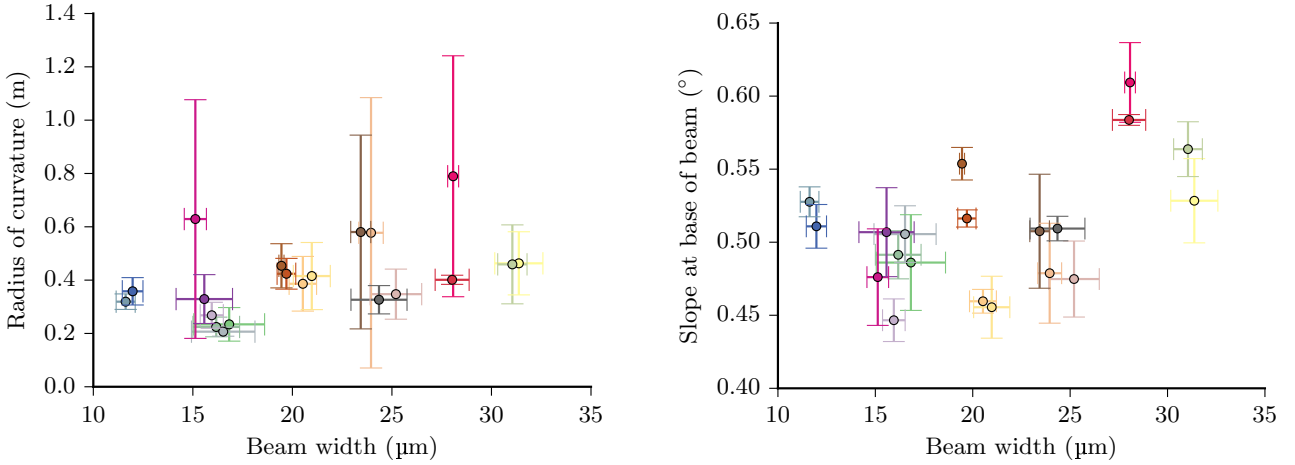

(a) Radius of curvature as function of beam width

(b) Slope at base of beam as function of beam width

Figure 10. The results of 20 measured waveguide beam arrays, each consisting of four beams. The mean value per array is presented by a circle and the error bars represent the standard deviation of the four beams within every array.

This non-uniformity might explain the differences from array to array (having different locations on the wafer), but not the differences within arrays. One would expect a high uniformity in SiO_2 thickness within a single array, considering the limited surface area of arrays (500 µm × 1000 µm). Further investigating the (non-)uniformity of SiO_2 thickness requires a more in-depth study and will be included in future work.

It should be mentioned that obtaining reliable deflection profiles is not easy, due to the fact that the SiO_2 waveguide beams are mostly transparent to white light. The measured profiles show deviations from a smooth line, and it is uncertain if these deviations exist in the beams or that they originate from the measurements. As an example, the deflection profile of a 1000 µm long, 28.4 µm wide beam is presented in figure 11. The step at a beam position of 850 µm is likely not a step in the top surface of the beam, but presumably results from the stitching operation performed by the profilometer to combine adjacent measurements.

The obtained radii and center coordinates of curve-fitted circles can be also used to obtain an estimate of the slope at the base of the beams. Figure 10(b) presents the slope at the base of the beam as a function of the beam width. Again, the mean values and the standard deviations of 20 arrays of four beams form the data points. The base slope varies from 0.45° to 0.61° over the 20 arrays. The variation in base slope within the arrays reveals a standard deviation of up to 0.04°.

Since the slope at the base of the beams is dependent on the SiO_2 thickness, the variation in base slope over the arrays can be explained by the variation in SiO_2 thickness over the wafer (i.e. 15.5 µm ± 0.7 µm). The slope variation within arrays is less likely caused by thickness non-uniformity, because of the limited surface area of arrays. This variation within arrays can be partly explained by the formation of a SiO_2 membrane at the base of the cantilevers. This membrane results from the fabrication process, and is created when Si underneath the SiO_2 is etched during the release of the beams. The boundary of the membrane is indicated in figure 8 by a dashed line. SiO_2 that is not supported by Si expands. At the membrane boundary, the SiO_2 is restricted at the Si - SiO_2 interface, and a downward slope is introduced in the SiO_2 membrane. Because the membrane is less flexible in the corners compared to the straight sections, the downward slope at the corners is smaller than at the straight sections. As a result, the two outer beams have a smaller downward slope than the two inner beams. This effect is in agreement with the measurement results.

4.3 Deflection over the length of the crossbar

The same optical profilometer was used to obtain the curvatures over the length of the crossbars. Measurements were performed on waveguide arrays consisting of four parallel beams connected at their free end by a crossbar.

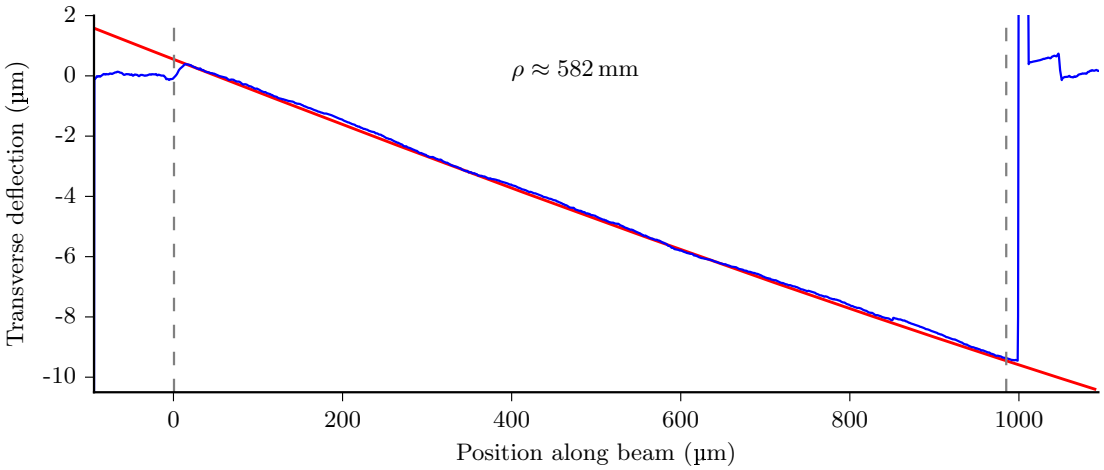

Figure 11. The deflection profile of a beam that is 1000 µm in length and 28.4 µm in width. The beam profile (shown in blue) deviates from the curve-fitted circle (shown in red).

Figure 12 shows two examples of the profile as measured over the crossbar of an array. The blue line represents the profile over the crossbar and the red line is a circle which is obtained by curve-fitting the profile. Please note that the profiles over the crossbar look more rough than the ones over the waveguide beams, because of the difference in scale of the vertical axis.

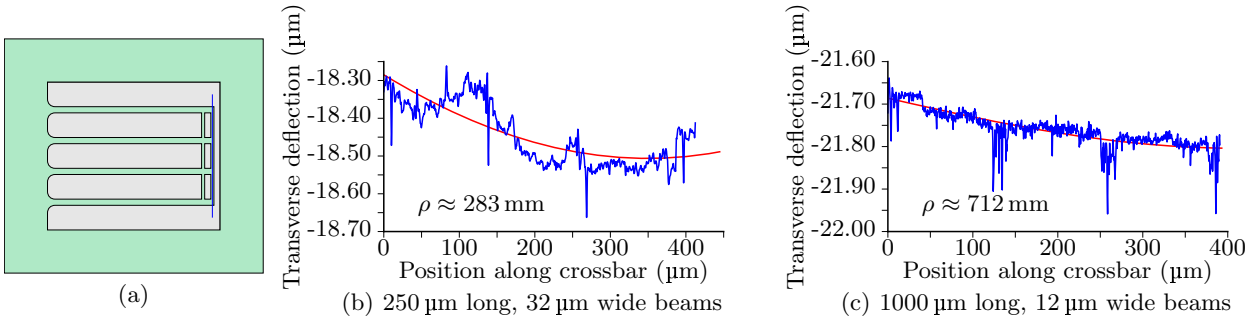

Figure 12. Example deflection profiles measured over the length of the crossbar. (a) shows how the profiles are measured over the length of the crossbar. (b), (c) The deflection profile is presented in blue. In red, a part of a circle is shown, obtained by curve-fitting the profile with a circle.

The radius of curvature of in total 16 crossbars is measured. We expect the curvature of crossbars to be dependent on the beam length. The bending stiffness reduces with increased beam length. As a result, the stiffness of the crossbar will be more dominant in case of longer beams. Figure 13 presents the measured radius of curvature of the crossbars as a function of beam length.

The radius of curvature of the measured crossbars ranges from 78 mm to 1304 mm. What is not visible in this plot, is that some crossbars (6 out of 23) have a concave downward curvature, as opposed to the concave upward curvature of the others. The number of measurements is small, making it difficult to draw conclusions based on this data. The occurrence of curvatures in both directions and the large deviations of the profiles from the curve-fitted circles suggest that the crossbar profiles do not follow a circular curvature.

An isolated crossbar, excluding any deformation caused by the waveguide beams, will theoretically have a slightly concave upward profile, similar to that of a single waveguide beam. If we include the influence of the waveguide beams, of which the inner two have a larger downward slope than the outer two, the crossbar should theoretically have a concave upward profile. The measured crossbar profiles are not exclusively concave upward,

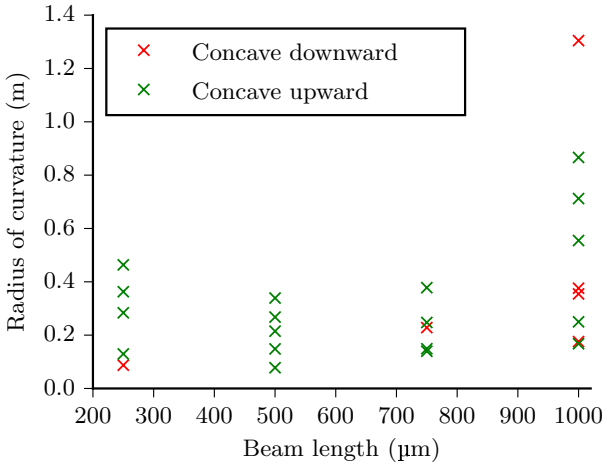

Figure 13. Radius of curvature measured over the length of the crossbar as a function of the beam length.

which is not in agreement with our expectation. But, as the beam measurements showed, there is a variation in width of the beams within a single array. This variation possibly affects the deformation profiles of the crossbars.

The variation in deflection within crossbars is in the order of tens of nanometer with a maximum of 200 nm. This is beneficial for the use of the waveguide arrays in the integrated alignment functionality. Preferably, crossbars are perfectly straight (when they are to be aligned with perfectly straight PICs). Small deflection variations within crossbars facilitate an accurate alignment of all the waveguides with the waveguides of straight PICs.

5. CONCLUSIONS AND PROSPECT

In this paper, we presented a fabrication method for suspended mechanically flexible waveguide arrays, based on TriPleX technology. The risk of the waveguide arrays fracturing was reduced by temporarily reinforcing the SiO_2 structure with supporting Si. The fabrication method was used to realize suspended waveguide arrays, which were mechanically characterized.

The overall yield of cantilevers was determined by optical inspection to be 96 %. Furthermore, the natural deformation of mechanically flexible waveguide structures was studied. The initial deformation over the length of the beams mainly results from a slope at the base of the beams of approximately 0.5°. Suspended waveguide beams show a slight concave upward curvature. The measured radius of curvature over the waveguide beams has a large spread and ranges from 0.2 m to 0.8 m. Crossbars do not follow a circular curvature, and the variation in deflection within crossbars is smaller than 0.2 µm. The characterization of the waveguide arrays provide useful information for applications of suspended TriPleX waveguides.

Follow-up research includes the integration of actuators for the positioning of the mechanically flexible waveguide arrays. The natural deformation profile will be different when another material is deposited on top of the suspended SiO_2 beams. Furthermore, optical characterization will be conducted to study the propagation of light through suspended waveguide beams.

ACKNOWLEDGMENTS

The research leading to the presented results has received funding from the STW Generic Technologies for Integrated Photonics (GTIP) programme, grant no. 11355 (Flex-O-Guides). We are grateful to Tom Scholtes and Johan van der Cingel of the Else Kooi Laboratory for the support in microfabrication. Furthermore, the support of Jaap Kokorian regarding the data analysis is highly appreciated.

REFERENCES

[1] Tekin, T., "Review of packaging of optoelectronic, photonic, and MEMS components," *Selected Topics in Quantum Electronics, IEEE Journal of* **17**, 704–719 (May 2011).

[2] Kopp, C., Bernab'e, S., Bakir, B., Fedeli, J.-M., Orobtchouk, R., Schrank, F., Porte, H., Zimmermann, L., and Tekin, T., "Silicon photonic circuits: On-CMOS integration, fiber optical coupling, and packaging," *Selected Topics in Quantum Electronics, IEEE Journal of* **17**, 498–509 (May 2011).

[3] Baehr-Jones, T., Pinguet, T., Lo Guo-Qiang, P., Danziger, S., Prather, D., and Hochberg, M., "Myths and rumours of silicon photonics," *Nature Photonics* **6**, 206–208 (Apr. 2012).

[4] Smit, M., Leijtens, X., Ambrosius, H., Bente, E., van der Tol, J., Smalbrugge, B., de Vries, T., Geluk, E.-J., Bolk, J., van Veldhoven, R., Augustin, L., Thijs, P., DAgostino, D., Rabbani, H., Lawniczuk, K., Stopinski, S., Tahvili, S., Corradi, A., Kleijn, E., Dzibrou, D., Felicetti, M., Bitincka, E., Moskalenko, V., Zhao, J., Santos, R., Gilardi, G., Yao, W., Williams, K., Stabile, P., Kuindersma, P., Pello, J., Bhat, S., Jiao, Y., Heiss, D., Roelkens, G., Wale, M., Firth, P., Soares, F., Grote, N., Schell, M., Debregeas, H., Achouche, M., Gentner, J.-L., Bakker, A., Korthorst, T., Gallagher, D., Dabbs, A., Melloni, A., Morichetti, F., Melati, D., Wonfor, A., Penty, R., Broeke, R., Musk, B., and Robbins, D., "An introduction to inp-based generic integration technology," *Semiconductor Science and Technology* **29**(8), 083001– (2014).

[5] Peters, T.-J., Tichem, M., and Staufer, U., "Suspended photonic waveguide arrays for submicrometer alignment," in [*SPIE Proceedings*], **9133**, 913317–1 – 913317–10 (2014).

[6] Fang, W. and Wickert, J. A., "Determining mean and gradient residual stresses in thin films using micromachined cantilevers," *Journal of Micromechanics and Microengineering* **6**(3), 301 (1996).

[7] Peters, T.-J. and Tichem, M., "Fabrication and characterization of suspended beam structures for SiO_2 photonic MEMS," *Journal of Micromechanics and Microengineering* **25**(10), 105003 (2015).

[8] Mohaupt, M., Beckert, E., Eberhardt, R., and Tünnermann, A., "Alignment procedures for micro-optics," in [*Precision Assembly Technologies and Systems*], Ratchev, S., ed., *IFIP Advances in Information and Communication Technology* **315**, 143–150, Springer Berlin Heidelberg (2010).

[9] Wörhoff, K., Heideman, R. G., Leinse, A., and Hoekman, M., "Triplex: a versatile dielectric photonic platform," *Advanced Optical Technologies* **4**(2), 189–207 (2015).